

# Physics prospects of second oscillation maximum at the Deep Underground Neutrino Experiment

Jogesh Rout<sup>§ a</sup>, Sheeba Shafaq<sup>§ b</sup>, Mary Bishai<sup>¶ c</sup>, and Poonam Mehta<sup>§ d</sup>

<sup>§</sup> *School of Physical Sciences, Jawaharlal Nehru University, New Delhi 110067, India*

<sup>¶</sup> *Brookhaven National Laboratory, PO Box 5000 Upton, NY 11973-5000*

December 22, 2024

## Abstract

Neutrino physics has entered a precision era and the unanswered questions at the present epoch relate to establishing the neutrino mass hierarchy, testing if there is CP violation in the leptonic sector, measuring the octant of  $\theta_{23}$  as well as to improve the resolution on the parameters of the mixing matrix including the CP phase. The precision measurement of neutrino parameters can be achieved by studying  $\nu_\mu \rightarrow \nu_e$  oscillations over a large  $L/E$  range. In the context of long baseline neutrino experiments (with fixed  $L$ ), this amounts to examining oscillations over a wide energy range. Most of the current and future long baseline experiments such as Deep Underground neutrino experiment (DUNE) are mainly sensitive to the neighbourhood of *first oscillation maximum* of the  $\nu_\mu \rightarrow \nu_e$  probability. In the present study, we elucidate the role of *second oscillation maximum* in investigating the sensitivity to the standard unknowns in oscillation physics. At the second oscillation maximum, one expects higher sensitivity to  $\delta$  as the size of the  $\delta$ -dependent interference term is a factor of  $\sim 3$  larger than that at the first oscillation maximum. We demonstrate that a beam tune optimized for coverage of the  $2^{nd}$  oscillation maxima at DUNE is possible using proposed accelerator upgrades that provide multi-MW of power at proton energies of 8 GeV. We perform sensitivity studies in the context of DUNE by utilising this new multi-MW 8 GeV beam tune in addition to wide-band beam tune that fully covers the region of the  $1^{st}$  oscillation maxima and part of the  $2^{nd}$ . We highlight the importance of second oscillation maximum in deciphering the intrinsic CP phase and also explore its impact on the precision measurement of the CP phase. We find that addition of the  $2^{nd}$  maxima beam tune to DUNE running with the standard wide-band CP optimized beam tune provides some improvement in sensitivity to the 3 flavor oscillation parameters. Further studies with improved detector resolution and beam optimizations will need to be carried out to fully exploit the capabilities of the  $2^{nd}$  maxima beam options at DUNE.

---

<sup>a</sup>Email: jogesh.rout1@gmail.com

<sup>b</sup>Email: sheebakhawaja7@gmail.com

<sup>c</sup>Email: mbishai@bnl.gov

<sup>d</sup>Email: pm@jnu.ac.in

# 1 Introduction

Pontecorvo's original insight that neutrinos oscillate among one another [1] has been confirmed by a variety of neutrino oscillation experiments involving wide range of energies and baselines. The idea of neutrino oscillations among the three light active neutrino flavours has been rewarded with a Nobel prize in 2015 [2]. The parameters entering the neutrino oscillation framework have been measured to a fairly good precision (see the recent global fit analyses [3, 4]). The best-fit values and  $3\sigma$  range of neutrino mass and mixings deciphered from oscillation data are given in Table 1. Yet, there are some open questions in the standard mass-induced oscillation framework. These include the question of neutrino mass hierarchy (sign of  $\Delta m_{31}^2$ ), the value of the CP violating phase ( $\delta$ ) and determining the correct octant of  $\theta_{23}$ . Furthermore, it is desirable to improve the precision measurements of the parameters entering the oscillation framework.

Determination of neutrino mass hierarchy (MH) would allow us to get closer towards determining the underlying structure of the neutrino mass matrix by being able to discriminate between theoretical models giving rise to neutrino masses [5]. Alongwith the CP violating phase  $\delta$ , it impacts the effectiveness of leptogenesis scenario which can explain the matter-antimatter asymmetry of the Universe [6].

The next generation neutrino oscillation experiments would allow us to precisely determine the known parameters and determine the remaining unknowns in the neutrino oscillation formalism. The long baseline neutrino experiments are designed such that the desirable physics outcome is achieved. Typically, the optimal combination is for a value of baseline ( $L$ ) and energy ( $E$ ) for which  $P_{\mu e}$  has its first peak. This is referred to as the *first oscillation maximum*. Typically, for shorter baselines, the higher oscillation maxima are inaccessible as the energies at which these occur are too small. For longer baselines, it may be possible to access the information from the *second (and higher) oscillation maxima*. At the second oscillation maximum, one expects higher sensitivity to  $\delta$  as the size of the  $\delta$ -dependent interference term is a factor of  $\sim 3$  larger than that at the first oscillation maximum.

A promising future experiment is the Deep Underground Neutrino Experiment (DUNE). Neutrino beam will be produced at Fermilab and will travel 1300 km to a liquid Argon (LAr) far detector placed at an on-axis location at Sanford Underground Research Facility (SURF). The primary aim of DUNE is to address the question of CP violation and identify the neutrino mass hierarchy [7–9]. A wide-band neutrino beam originating from the Fermilab proton complex is considered for DUNE. A systematic evaluation of optimal baseline for discovery of CP violation, determination of the mass hierarchy and resolution of the  $\theta_{23}$  octant in a long baseline oscillation experiment was carried out by Bass et al. [10] and it was concluded that for achieving unambiguous measurement of these parameters, one needed a baseline atleast of the order of 1000 km. It was further shown from the asymmetry plot that CP measurement was better achieved in the vicinity of second oscillation maximum irrespective of the mass hierarchy and results for sensitivities to standard three flavour oscillation parameters were presented. The authors had considered two detector types - Water Cherenkov (WC) and LAr and performed the study for the erstwhile Long Baseline Neutrino Experiment (LBNE).

The idea of utilizing the second oscillation maximum in neutrino experiments is not new.

Parameter	Best-fit value	$3\sigma$ range	$3\sigma$ uncertainty [%]
$\theta_{12}$ [°]	34.3	31.4 - 37.4	8.72
$\theta_{13}$ (NH) [°]	8.58	8.16 - 8.94	4.56
$\theta_{13}$ (IH) [°]	8.63	8.21 - 8.99	4.53
$\theta_{23}$ (NH) [°]	48.8	41.63 - 51.32	10.42
$\theta_{23}$ (IH) [°]	48.8	41.88 - 51.30	10.11
$\Delta m_{21}^2$ [eV <sup>2</sup> ]	$7.5 \times 10^{-5}$	$[6.94 - 8.14] \times 10^{-5}$	8.0
$\Delta m_{31}^2$ (NH) [eV <sup>2</sup> ]	$+2.56 \times 10^{-3}$	$[2.46 - 2.65] \times 10^{-3}$	3.72
$\Delta m_{31}^2$ (IH) [eV <sup>2</sup> ]	$-2.46 \times 10^{-3}$	$-[2.37 - 2.55] \times 10^{-3}$	3.7
$\delta$ (NH) [Rad]	$-0.8\pi$	$[-\pi, 0] \cup [0.8\pi, \pi]$	—
$\delta$ (IH) [Rad]	$-0.46\pi$	$[-0.86\pi, -0.1\pi]$	—

**Table 1:** Standard oscillation parameters and their uncertainties used in our study. The values were taken from the global fit analysis in [3]. If the  $3\sigma$  upper and lower limit of a parameter is  $x_u$  and  $x_l$  respectively, the  $3\sigma$  uncertainty is  $(x_u - x_l)/(x_u + x_l)\%$ .

The prospect of using high intensity low energy neutrino beam using Project X was studied in [11] and it was demonstrated that the simultaneous operation of 8 GeV and 60 GeV beams in conjunction with a WC detector allows for sensitivity to  $\nu_\mu \rightarrow \nu_e$  oscillation at the second oscillation maximum. The focus of the study was to attain high precision measurement of  $\theta_{13}$  and  $\delta_{CP}$ . With the goal of enhancing the mass hierarchy sensitivity, the authors of [12] introduced a second detector at an off-axis location (same beam was used) and obtained marginal improvement for certain values of  $\delta_{CP}$  in the worse half plane of  $\delta_{CP}$  values. In [13], the idea of utilizing different oscillation maxima was invoked in discussing the role and interplay between appearance and disappearance channels at long baseline experiments for precision measurement of  $\delta$  and  $\theta_{23}$ . In [14], for the considered experimental setup (Fermilab to DUSEL LBNE), it was concluded that the second maximum plays only a marginal role due to the experimental difficulties to obtain a statistically significant and sufficiently background-free event sample at low energies. The European Spallation Source (ESS) neutrino Super Beam (ESS $\nu$ SB) facility in Europe utilizes the second oscillation peak to maximize the discovery potential to leptonic CP violation with the detector placed at  $L = 540$  km. The  $L/E$  is such that the second oscillation peak can naturally be exploited in order to measure oscillation parameters [15–21]. Among other experiments, the MOMENT [22] proposal ( $L = 150$  km) has similar  $L/E$  as the ESS $\nu$ SB. The prospect of precision measurement of  $\delta$  at MOMENT has been studied in [23]. The T2HKK [24] proposal, in which the first and the second oscillation maxima are measured with two detectors located at different sites will have the same  $L/E$  range. More recently, invisible neutrino decay at ESS $\nu$ SB has been explored in [25] and a comparative analysis of T2HK, T2HKK and ESS $\nu$ SB in the context of neutrino decay has been carried out in [26].

However, it should be noted that, a comprehensive and detailed assessment of the role of different oscillation maxima for long baseline experiment such as DUNE has not been addressed in the earlier work and this is the main motivation of the present study. In the present article, we begin with a probability level analysis highlighting the role of second

oscillation maxima and its impact on the current unknowns in neutrino oscillation physics. We also address the issue of extraction of intrinsic CP violation using the two beams and show that the second oscillation maximum helps in resolving the ambiguity in CP phase measurement. We utilize optimal beam tunes to explore the precise role of first and second oscillation maxima. The standard beam tune used in almost all the studies connected with DUNE sensitivities is derived from 80 GeV proton beam energy and this is well-suited to optimize signal from the first oscillation maximum. However, one needs a different source to utilize the second oscillation maximum - here we employ an 8 GeV beam as was proposed in Project X [11] to harness the signal at second oscillation maximum.

The present article is structured as follows. In Sec. 2, we describe the basic framework used in the present work. This includes a review of electron neutrino appearance probability in vacuum and in matter, oscillation maxima of  $P_{\mu e}$ , CP asymmetry, mass hierarchy (MH) asymmetry and a description of an observable for separation of intrinsic versus extrinsic contribution to the CP phase. In Sec. 3.2, we describe the experimental inputs such as beam tunes used and detector details. Sec. 4 is devoted to a discussion at the level of event rates (with a discussion on backgrounds) at DUNE using different beam tunes. In Sec. 6, we present our main results for sensitivities to CP, mass hierarchy, octant of  $\theta_{23}$ , resolution of  $\delta$  and  $1\sigma$  contours from a two-dimensional fit to  $\theta_{23}$  and  $\delta$  at the level of  $\chi^2$ . We summarize our outcome in Sec. 7.

## 2 Framework

Neutrino oscillations have their origin in the non-zero neutrino masses and mixing among the neutrino flavors. The standard paradigm of neutrino oscillations involves three flavours of neutrinos which are superpositions of the mass states carrying well-defined masses. The mixing matrix ( $\mathcal{U}$ ) in the Pontecorvo-Maki-Nakagawa-Sakata (PMNS) parametrization [27] is given by

$$\mathcal{U} = \begin{pmatrix} 1 & 0 & 0 \\ 0 & c_{23} & s_{23} \\ 0 & -s_{23} & c_{23} \end{pmatrix} \begin{pmatrix} c_{13} & 0 & s_{13}e^{-i\delta} \\ 0 & 1 & 0 \\ -s_{13}e^{i\delta} & 0 & c_{13} \end{pmatrix} \begin{pmatrix} c_{12} & s_{12} & 0 \\ -s_{12} & c_{12} & 0 \\ 0 & 0 & 1 \end{pmatrix}, \quad (1)$$

where  $s_{ij} = \sin \theta_{ij}$ ,  $c_{ij} = \cos \theta_{ij}$  and  $\delta$  is the Dirac-type CP phase. Additionally, if neutrinos are Majorana, there can be two additional Majorana-type phases in the three flavour case. However, those Majorana phases play no role in neutrino oscillations [28].

In a typical long baseline experiment such as DUNE, at the source, neutrinos are produced via pion decay process and in the muon flavour. In principle, all the oscillation channels  $\nu_\mu \rightarrow \nu_e$  ( $\nu_e$  appearance),  $\nu_\mu \rightarrow \nu_\mu$  ( $\nu_\mu$  disappearance) and  $\nu_\mu \rightarrow \nu_\tau$  ( $\nu_\tau$  appearance) should be accessible at DUNE. However, with the standard beam tune of the LBNF beamline, the  $\nu_\mu \rightarrow \nu_\tau$  appearance channel does not lead to sizable event samples [29] and it is not possible to probe this channel. In recent studies, it has been shown that higher energy beam tunes may prove useful to probe this channel [30–32]. However, here, we are concerned with the standard beam tune at DUNE and the flux relevant for the 2<sup>nd</sup> maxima, so the channels considered are :  $\nu_e$  appearance channel and  $\nu_\mu$  disappearance channel. In order to have a clear understanding of the role of second oscillation maximum vis a vis the first

oscillation maximum in probing the current unknowns, we briefly describe the main features of oscillation probability for  $\nu_\mu \rightarrow \nu_e$  channel.

## 2.1 Brief review of $P_{\mu e}$ in vacuum and in matter

For propagation of neutrinos through vacuum,  $P_{\mu e}^v$  can be expressed as (see [33]).

$$P_{\mu e}^v \simeq P_0^v + P_{\sin \delta}^v + P_{\cos \delta}^v + P_3^v, \quad (2)$$

where

$$P_0^v = \sin^2 \theta_{23} \sin^2 2\theta_{13} \sin^2 \Delta_{31}, \quad (3a)$$

$$P_{\sin \delta}^v = \sin \delta \cos \theta_{13} \sin 2\theta_{12} \sin 2\theta_{13} \sin 2\theta_{23} \sin^2 \Delta_{31} \sin(2\alpha \Delta_{31}), \quad (3b)$$

$$P_{\cos \delta}^v = \cos \delta \cos \theta_{13} \sin 2\theta_{12} \sin 2\theta_{13} \sin 2\theta_{23} \sin \Delta_{31} \sin(2\alpha \Delta_{31}) \cos \Delta_{31}, \quad (3c)$$

$$P_3^v = \cos^2 \theta_{23} \sin^2 2\theta_{12} \sin^2(\alpha \Delta_{31}). \quad (3d)$$

Here  $\Delta_{31} = \Delta m_{31}^2 L/4E$  and  $\alpha = \Delta m_{21}^2/\Delta m_{31}^2$ .  $E$  is the neutrino energy in GeV and  $L$  is the baseline in km. For antineutrinos,  $\delta \rightarrow -\delta$ . Here  $P_0^v$  is the dominant term (Eq. 3a). The CP phase dependence lies in two interference terms,  $P_{\sin \delta}^v$  and  $P_{\cos \delta}^v$  (see Eq. 3b and 3c).  $P_{\sin \delta}^v$  is the CP violating term as it changes sign for antineutrinos, while the  $P_{\cos \delta}^v$  is the CP conserving term. It is clear that both  $\Delta m_{21}^2$  and  $\Delta m_{31}^2$  are required to be non-zero in order to extract any information about the CP phase.  $P_3^v$  is a relatively smaller term (Eq. 3d).

In presence of standard interactions with matter, Eq. 2 and Eq. 3 are no longer applicable and it is tedious to obtain approximate analytic expressions. It becomes imperative to use certain approximations to derive an analytical expression for  $P_{\mu e}^m$ . One typically uses constant density approximation and also the fact that  $\alpha$  and  $\theta_{13}$  are small parameters so that one can employ perturbation techniques to obtain an expression (valid upto second order) for  $P_{\mu e}^m$  (see [34–36]). Here again, we can write down the approximate expression for probability as a sum of four terms which are modified in presence of matter.

$$P_{\mu e}^m \simeq P_0^m + P_{\sin \delta}^m + P_{\cos \delta}^m + P_3^m, \quad (4)$$

where

$$P_0^m = \sin^2 \theta_{23} \frac{\sin^2 2\theta_{13}}{(\hat{A} - 1)^2} \sin^2((\hat{A} - 1)\Delta_{31}), \quad (5a)$$

$$P_{\sin \delta}^m = \alpha \frac{\sin \delta \cos \theta_{13} \sin 2\theta_{12} \sin 2\theta_{13} \sin 2\theta_{23}}{\hat{A}(1 - \hat{A})} \sin(\Delta_{31}) \sin(\hat{A}\Delta_{31}) \sin((1 - \hat{A})\Delta_{31}), \quad (5b)$$

$$P_{\cos \delta}^m = \alpha \frac{\cos \delta \cos \theta_{13} \sin 2\theta_{12} \sin 2\theta_{13} \sin 2\theta_{23}}{\hat{A}(1 - \hat{A})} \cos(\Delta_{31}) \sin(\hat{A}\Delta_{31}) \sin((1 - \hat{A})\Delta_{31}), \quad (5c)$$

$$P_3^m = \alpha^2 \frac{\cos^2 \theta_{23} \sin^2 2\theta_{12}}{\hat{A}^2} \sin^2(\hat{A}\Delta_{31}), \quad (5d)$$

where  $\hat{A} = A/\Delta m_{31}^2$  where  $A = 2VE = 2\sqrt{2}G_F n_e E = 2 \times 0.76 \times 10^{-4} \times Y_e \times [\rho/g \text{ cm}^{-3}] \times [E/GeV] \text{ eV}^2$  is the Wolfenstein term.  $G_F$  is the Fermi constant and  $n_e$  is the electron

number density in Earth matter ( $n_e = N_{Av} Y_e \rho$  where,  $N_{Av}$  is the Avogadro's number,  $Y_e$  is the electron fraction and  $\rho$  is Earth matter density). For antineutrinos,  $\delta \rightarrow -\delta$  and  $A \rightarrow -A$ . The above expression is valid only when  $\alpha \Delta_{31} \lesssim 1$  which in turn means that the expression would give reasonable results for  $E > 0.8$  GeV for baselines below 8,000 km [35].

Note that,  $P_0^m$  is the dominant term as it is independent of  $\alpha$  (Eq. 5a). We note that the  $\delta$ -dependent interference terms (Eq. 5b and 5c) are suppressed by the hierarchy parameter,  $\alpha$  and the last term,  $P_3^m$  is proportional to  $\alpha^2$  (Eq. 5d).

## 2.2 First and second oscillation maxima of $P_{\mu e}$

Since the leading term depends on  $\Delta_{31}$ , the physical characteristics of an appearance experiment are therefore determined by the baseline ( $L$ ) and neutrino energy ( $E$ ) at which the mixing between the  $\nu_1$  and  $\nu_3$  states is maximal. If we look at the leading oscillatory term of  $P_{\mu e}^v$ , we get oscillation maxima at

$$\begin{aligned} \frac{\Delta m_{31}^2 L}{4E} &= (2n - 1) \frac{\pi}{2} \\ \frac{L}{E} &= (2n - 1) \frac{\pi}{2} \left( \frac{1}{1.267} \right) \left( \frac{2.56 \times 10^{-3} \text{ eV}^2}{\Delta m_{31}^2} \right) \\ \implies \frac{L}{E} &\simeq (2n - 1) \times 500 \frac{\text{km}}{\text{GeV}} \end{aligned} \quad (6)$$

where  $n$  is an integer and  $n = 1, 2, \dots$  stands for first, second, ... oscillation maxima occurring at  $L/E \simeq 500, 1500, \dots$  km/GeV and so on. For a fixed baseline of 1300 km, this would imply  $E^I \simeq 2.6$  GeV and  $E^{II} \simeq 0.87$  GeV for first and second oscillation maxima respectively. It may be possible to observe the higher ( $n > 1$ ) oscillation maximas when the baselines are comparatively longer (so that the energies at which higher maxima occur are not too small). A useful observable to understand the impact of CP phase on the oscillation probabilities (Eqs. 3 and 5) is the CP asymmetry [37] and in the next subsection we examine the analytic expression for the CP asymmetry in vacuum and in matter.

## 2.3 CP Asymmetry in vacuum and in matter

The CP asymmetry is given by

$$A_{\mu e}^{CP} = \frac{P_{\mu e}(\delta) - \bar{P}_{\mu e}(\delta)}{P_{\mu e}(\delta) + \bar{P}_{\mu e}(\delta)} = \frac{\Delta P_{\mu e}^{CP}}{\sum P_{\mu e}^{CP}} \quad (7)$$

Since CP asymmetry is a ratio of probabilities, the systematic uncertainties mostly cancel out at the level of event rates. In vacuum, the numerator is given by <sup>1</sup>

$$\begin{aligned} \Delta P_{\mu e}^{CP} &= 8J[\sin(2\alpha\Delta_{31}) \sin^2(\Delta_{31}) - \sin(2\Delta_{31}) \sin^2(\alpha\Delta_{31})] , \\ &= \underbrace{16 \sin \delta J_r [\sin(\Delta_{31}) \sin(\alpha\Delta_{31}) \sin(1 - \alpha)\Delta_{31}]}_{\text{intrinsic}} , \end{aligned} \quad (8)$$

<sup>1</sup>Eq. 8 is obtained by using the exact three flavour formula for  $P_{\mu e}$  in vacuum given in [38].

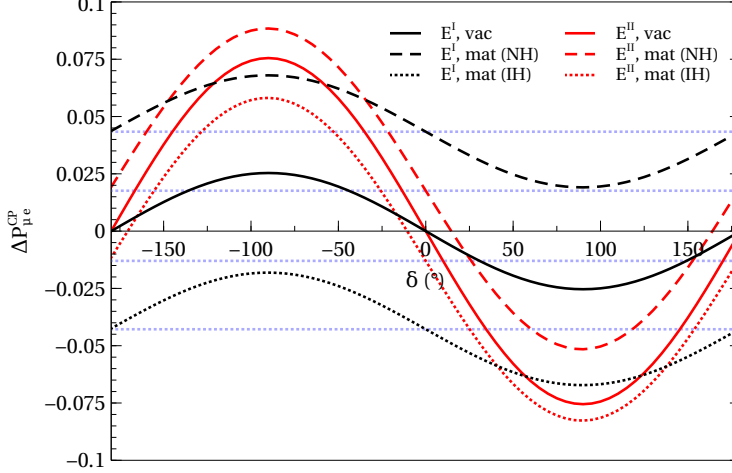


**Figure 1:**  $\Delta P_{\mu e}^{CP}$  plotted in vacuum (solid lines) and in matter (dashed lines for NH and dotted lines for IH) as a function of  $\delta$  for a fixed baseline of 1300 km.  $E^I \simeq 2.6$  GeV and  $E^{II} \simeq 0.87$  GeV refer to the first (black) and second (red) oscillation maxima respectively.

where  $J = \sin \theta_{12} \cos \theta_{12} \sin \theta_{23} \cos \theta_{23} \sin \theta_{13} \cos^2 \theta_{13} \sin \delta = J_r \sin \delta$  is the measure of CP violation and is referred to as the Jarlskog factor [39]. In vacuum, therefore, if the CP phase  $\delta$  is either 0 or  $\pi$ , the CP asymmetry vanishes. However, matter effects can create a fake CP asymmetry. In case of matter, we have

$$\begin{aligned} \Delta P_{\mu e}^{CP} &\approx \underbrace{\sin^2 \theta_{23} \sin^2 2\theta_{13} \Theta_+ \Theta_-}_{\text{extrinsic}} \\ &+ \underbrace{8\alpha J_r \frac{\sin(\hat{A}\Delta_{31})}{\hat{A}} [\cos \delta \Theta_- \cos \Delta_{31} + \sin \delta \Theta_+ \sin \Delta_{31}]}_{\text{intrinsic and extrinsic}}, \end{aligned} \quad (9)$$

where  $\Theta_{\pm} = \sin[(\hat{A} - 1)\Delta_{31}]/(\hat{A} - 1) \pm \sin[(\hat{A} + 1)\Delta_{31}]/(\hat{A} + 1)$ . The presence of first term implies that one will have a non-vanishing contribution to  $\Delta P_{\mu e}^{CP}$  due to the MSW matter effect [40, 41] since  $\hat{A} \rightarrow -\hat{A}$  for antineutrinos. From Eq. 9, we note that the  $\cos \delta$  dependent term is proportional to  $\cos \Delta_{31}$ . This implies that at location of oscillation maxima ( $\cos \Delta_{31} = 0$ ), the  $\cos \delta$  term vanishes.

In Fig. 1, we plot the probability difference as a function of  $\delta$  for a fixed values of energy corresponding to first and second oscillation maxima and baseline of 1300 km (for DUNE). The curves are plotted in vacuum and in matter (see Eq. 8 and Eq. 9). The following comments are in order.

- From Eq. 8, we note that  $\Delta P_{\mu e}^{CP} \propto \sin \delta$  in vacuum. While there is a  $\cos \delta$  term in presence of matter (Eq. 9), it vanishes (at the location of first and second oscillation maxima as  $\cos \Delta_{31} \rightarrow 0$ ) and  $\delta$  dependence is via the  $\sin \delta$  term in matter as well.
- $\Delta P_{\mu e}^{CP}$  at  $E^{II} > \Delta P_{\mu e}^{CP}$  at  $E^I$  both in vacuum and in matter. The largest difference occurs around  $\delta = \pm 90^\circ$ . At  $\delta = -90^\circ$ , in vacuum,  $\Delta P_{\mu e}^{CP} \simeq 0.025$  at  $E^I$ ;  $\Delta P_{\mu e}^{CP} \simeq 0.075$  at  $E^{II}$ . In matter (for NH),  $\Delta P_{\mu e}^{CP} \simeq 0.07$  at  $E^I$  and  $\Delta P_{\mu e}^{CP} \simeq 0.088$  at  $E^{II}$ .

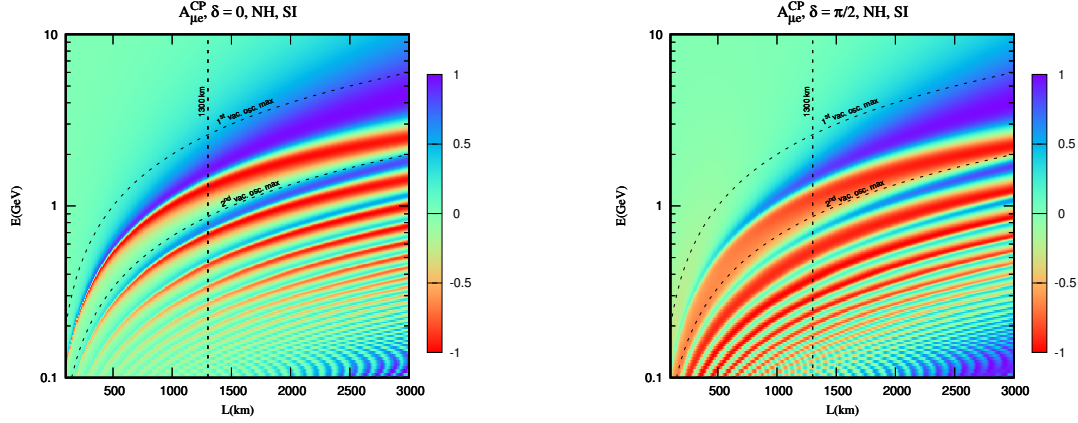


**Figure 2:** Oscillogram of CP asymmetry in the plane of  $E$  and  $L$  for  $\delta = 0$  and  $\delta = \pi/2$ .

- For CP conserving values i.e.,  $\delta = 0^\circ$  or  $180^\circ$ , in vacuum  $\Delta P_{\mu e}^{CP}$  vanishes at  $E^I$  and  $E^{II}$ . But, in matter (for NH),  $\Delta P_{\mu e}^{CP} \neq 0$  due to matter effects (pure extrinsic) and in fact,  $\Delta P_{\mu e}^{CP} \simeq 0.043$  at  $E^I$  and  $\Delta P_{\mu e}^{CP} \simeq 0.017$  at  $E^{II}$ .
- In general, when  $\delta \neq 0$ , the extrinsic effects complicate the determination of intrinsic CP phase. As matter effects are more pronounced at  $E^I$  than at  $E^{II}$ , the intrinsic versus extrinsic separation is harder at  $E^I$  than at  $E^{II}$ .
- The main advantage of studies at second maximum over the first maximum lies in our ability to extract the intrinsic CP component better than that with first maximum. This is due to the fact that CP asymmetry in vacuum is larger while the matter effects are not as large.

In order to explore the features of second oscillation maximum versus the first oscillation maximum as a function of  $E$  and  $L$ , in Fig. 2, we show oscillograms of CP asymmetry in the plane of  $E$  and  $L$ . The location of first and second oscillation maxima in the plane of  $E$  and  $L$  is depicted in the plots. For  $\delta = 0$  (left panel), the asymmetry at second maximum is very small, as expected. However, matter effects play a crucial role at first maximum as can be seen for baselines beyond  $L \approx 1000$  km and the CP asymmetry grows with  $L$ . However, for  $\delta = \pi/2$  (right panel), the intrinsic contribution to CP asymmetry is maximal. Moreover, there is additional extrinsic CP contribution (matter-induced) and one can see significant change in the CP asymmetry at second oscillation maximum independent of the baseline. The CP asymmetry has opposite sign (red) in comparison to CP asymmetry at first oscillation maximum (blue). This is consistent with Fig. 1 near  $\delta \simeq \pi/2$  for 1300 km.

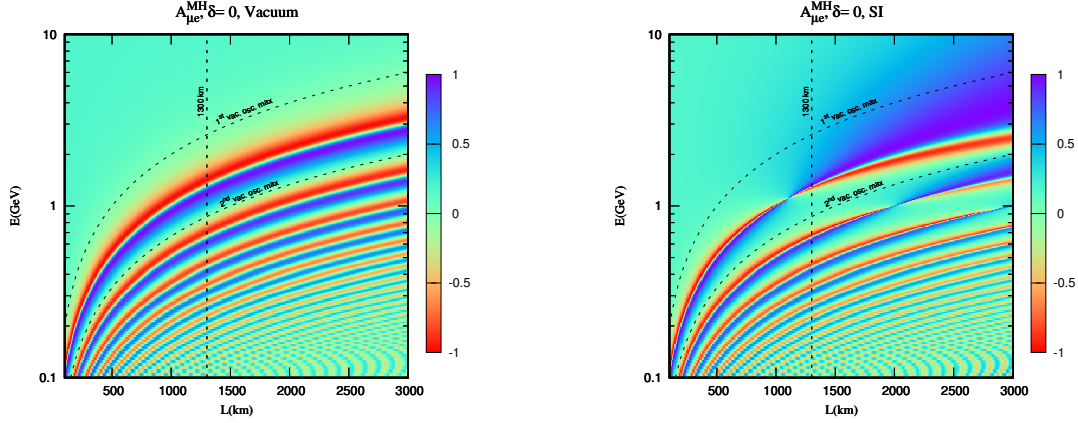


**Figure 3:** Oscillogram of MH asymmetry in the plane of  $E$  and  $L$  for  $\delta = 0$  in vacuum (left) and matter (right).

## 2.4 Mass hierarchy asymmetry in vacuum and in matter

The MH asymmetry is given by

$$A_{\mu e}^{MH} = \frac{P_{\mu e}^{NH} - P_{\mu e}^{IH}}{P_{\mu e}^{NH} + P_{\mu e}^{IH}} = \frac{\Delta P_{\mu e}^{MH}}{\sum P_{\mu e}^{MH}} \quad (10)$$

In vacuum,

$$\Delta P_{\mu e}^{MH} \approx 2J_r \sin \Delta_{31} \sin \Delta_{21} \cos \Delta_{31} (\cos \delta \cos \Delta_{21} - 8 \sin \delta \sin \Delta_{21}) \quad (11)$$

In matter,

$$\Delta P_{\mu e}^{MH} \approx \sin^2 \theta_{23} \sin^2 2\theta_{13} \Theta_+ \Theta_- + 8\alpha J_r \frac{\sin(\hat{A}\Delta_{31})}{\hat{A}} [\cos \delta \Theta_+ \cos \Delta_{31} + \sin \delta \Theta_- \sin \Delta_{31}] \quad (12)$$

where  $\Theta_{\pm} = \sin[(\hat{A} - 1)\Delta_{31}]/(\hat{A} - 1) \pm \sin[(\hat{A} + 1)\Delta_{31}]/(\hat{A} + 1)$  as given before.

In Fig. 3, we show oscillograms for the MH asymmetry for  $\delta = 0$  in the plane of  $E$  and  $L$  for vacuum (left) and matter (right). The  $\Delta P_{\mu e}^{MH}$  is expected to vanish at all nodes (maxima and minima) since  $\Delta P_{\mu e}^{MH} \propto \cos \Delta_{31} \sin \Delta_{31}$  in vacuum (Eq. 11). This is independent of the value of  $\delta$  (Fig. 3, left panel). From the left panel of Fig. 3, we note that the MH asymmetry is vanishingly small at both the oscillation maxima. If we examine the right panel of Fig. 3, at first oscillation maximum, one expects large matter induced changes in probability in comparison to vacuum which aids the determination of neutrino MH provided the baseline is long enough for matter effects to be substantial.

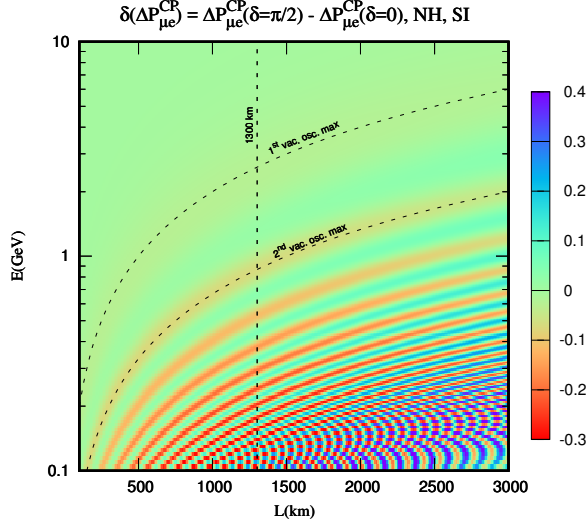


**Figure 4:** Oscillogram in the plane of  $E$  and  $L$  depicting separation of the intrinsic CP contribution from the extrinsic CP contribution.

## 2.5 Distinguishing between intrinsic and extrinsic CP contribution

In presence of matter, the CP asymmetry can be expressed in terms of intrinsic and extrinsic CP factors (see Eq. 9). The issue of separation of intrinsic contribution from the extrinsic contribution has been addressed in [42, 43] and a useful observable (matter contribution gets approximately cancelled) to disentangle the two contributions was suggested. The observable is given by

$$\delta(\Delta P_{\mu e}^{CP}) = \Delta P_{\mu e}^{CP}(\delta = \pi/2) - \Delta P_{\mu e}^{CP}(\delta = 0) \quad (13)$$

Using this observable, we next depict an oscillogram in the plane of  $E$  and  $L$  to illustrate separation of the intrinsic versus extrinsic CP contribution in Fig. 4. It is clear that the second oscillation maximum allows for a clean extraction of the intrinsic CP phase. This can be easily explained by Fig. 1, from which we noted that matter influences the probability at first oscillation maximum far more than it impacts the probability at the location of second oscillation maximum. This point and the fact that the intrinsic CP asymmetry is larger at second oscillation maximum makes the second oscillation maximum the preferred option for addressing the question of separating the intrinsic contribution to the CP phase.

Our discussion, thus far, has been at the level of probabilities and in order to obtain realistic quantitative results, one needs to check the outcome at the level of event rates. The following section covers the experimental details used in our simulations.

### 3 Experimental inputs

#### 3.1 Beam tunes used

The fluxes considered in the present work are plotted as a function of energy in Fig. 5.

- **LE flux** : The standard wideband beam used in almost all studies of DUNE is derived from proton beam of energy 80 GeV [8,44]. By virtue of its wideband nature, the LE beam is also sensitive to regions above and below the first oscillation maximum.
- **2<sup>nd</sup> maxima flux** : The neutrino beam at the 2<sup>nd</sup> maxima is obtained using a 3 MW, 8 GeV proton beam which could be generated by the PIP-III superconducting linac option [45].

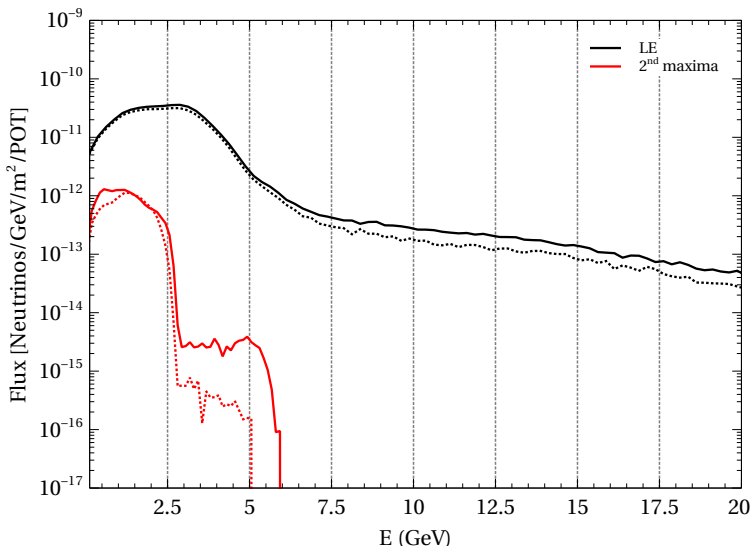


**Figure 5:** The fluxes used in the present study. The LE flux corresponds to the 80 GeV, 1.1 MW beam (as used in Conceptual Design Report (CDR) [8]) and the 2<sup>nd</sup> maxima flux is the 8 GeV, 3MW beam. The solid line corresponds to the neutrino mode while the dotted line corresponds to the antineutrino mode.

The beamline details for the two fluxes are listed in Table 2.

#### 3.2 Detector details

The DUNE far detector (FD) is described in detail in Volume 4 [47] of the DUNE CDR. In our analysis, we have assumed that a Liquid Argon (LAr) far detector of fiducial mass 40 kt situated at a distance of 1300 km. We have combined both electron neutrino appearance ( $\nu_\mu \rightarrow \nu_e$ ) and muon neutrino disappearance ( $\nu_\mu \rightarrow \nu_\mu$ ) channels, both in neutrino and anti-neutrino mode. Details of the experimental configuration and other parameters relevant for DUNE are given in Table 3.

Parameter	LE (CPV optimized design)	2 <sup>nd</sup> maxima
Proton beam energy	80 GeV	8 GeV
Proton Beam power	1.1 MW (2.2 MW)	3 MW
Protons on target (POT) per year	$1.47 \times 10^{21}$ ( $2.94 \times 10^{21}$ )	$40.1 \times 10^{21}$
Focussing	2 horns, GA optimization (2015 conceptual design)	2 horns, GA optimization (2015 conceptual design)
Horn Current	$\sim 300$ kA	$\sim 300$ kA
Decay pipe length	194 m	200 m
Decay pipe diameter	4 m	4 m

GA  $\rightarrow$  Genetic Algorithm

**Table 2:** Beamline parameters assumed for the different design fluxes used in our sensitivity calculations [7, 11, 46]. The LBNF neutrino beamline decay pipe length has been chosen to be 194 m.

S. No.	Relevant parameter	DUNE
1	Location	USA
2	Status	under construction
3	Accelerator facility	Fermilab
4	Beam power	1.1 MW, 2.2 MW, 3 MW
5	Expected POT	$1.47 \times 10^{21}$ , $2.9 \times 10^{21}$ , $40.1 \times 10^{21}$
6	Baseline length	1300 km
7	Off-axis angle	0°
8	Detector technology	LAr
9	Fiducial mass	40 kton
10	Run times	5 yr with 1.1 MW + 5 yr with 2.2 MW + 5 yr with 3 MW
11	Energy window (GeV)	[0.5,18.0]
12	Energy bins	71
13	Energy resolution, $\sigma_e$	migration matrices
14	Normalization error	$\nu_e$ : 2% (signal) $\nu_e$ : 5% (bkgd) $\nu_\mu$ : 5% (signal) $\nu_\mu$ : 5% (bkgd)

**Table 3:** Details of the experimental configuration and other parameters relevant for DUNE.

## 4 Event spectrum at DUNE

In order to simulate DUNE, we use the GLoBES package [48, 49] with the recent DUNE configuration file provided by the collaboration [46]. We implement the density profile of Earth as given by Preliminary Reference Earth Model (PREM) [50]. The impact of improved neutrino energy reconstruction capabilities at DUNE (at first oscillation maximum only) has been studied in [51].

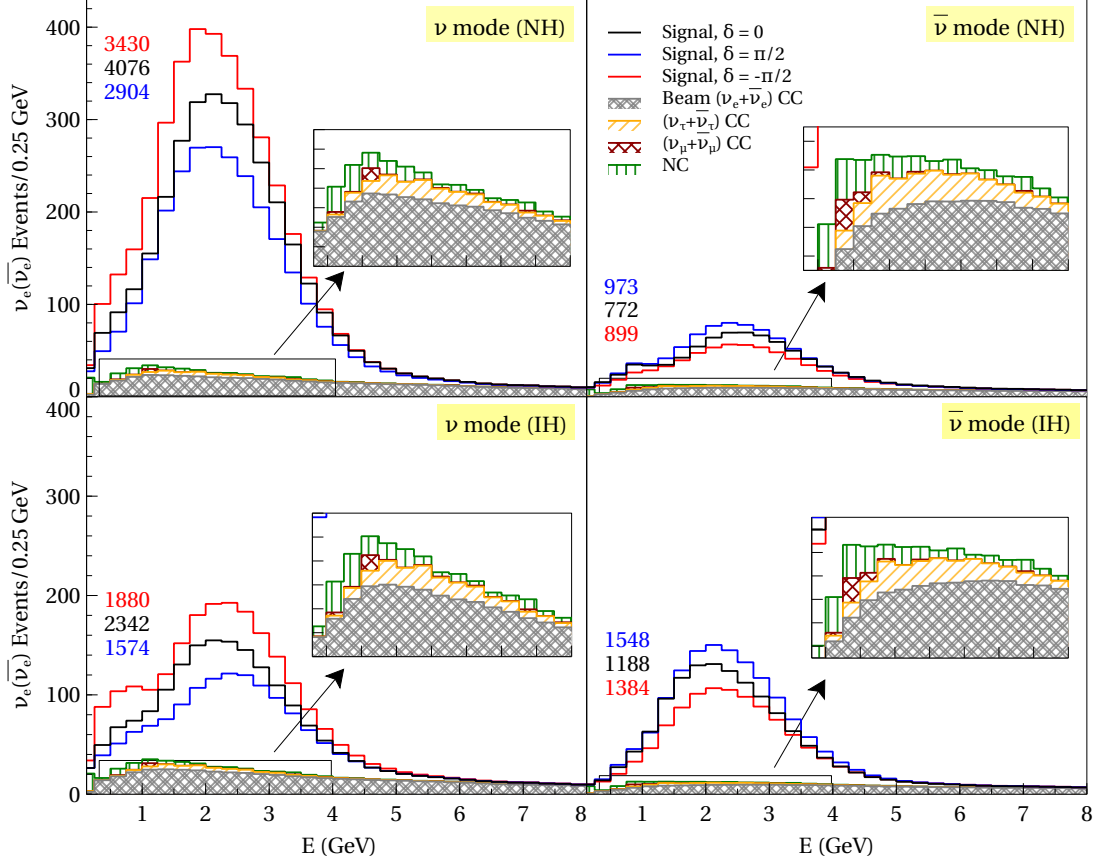


**Figure 6:** Electron (anti-)neutrino appearance event spectrum with a 40 kt DUNE far detector for the beam combination : LE 1.1 MW beam, LE 2.2 MW beam and  $2^{nd}$  maxima 3 MW beam for different values of  $\delta$  ( $\delta = 0, \pi/2, -\pi/2$ ). The runtime of 15 yr is split equally among the three beams (5 yr each) and distributed evenly between neutrino and antineutrino modes (2.5 yr +2.5 yr) for each beam tune. The event rates are stacked from below backgrounds. The total number of events corresponding to a particular value of  $\delta$  are mentioned in each panel.

We consider the following beam and runtime combinations :

- (a) LE, 1.1 MW + LE, 2.2 MW  $\rightarrow$  runtime of 5 yr in LE, 1.1 MW and 5 yr in LE, 2.2 MW distributed equally in neutrino and antineutrino modes
- (b)  $2^{nd}$  maxima, 3 MW  $\rightarrow$  runtime of 5 yr distributed equally in neutrino and antineutrino modes
- (c) LE, 1.1 MW + LE, 2.2 MW +  $2^{nd}$  maxima, 3 MW  $\rightarrow$  runtime of 5 yr in LE, 1.1 MW, 5 yr in LE, 2.2 MW and 5 yr with  $2^{nd}$  maxima, 3 MW distributed equally in neutrino and antineutrino modes

Table 4 lists the total signal and background events for the three beam combinations mentioned above for the  $\nu_e$  appearance and  $\nu_\mu$  disappearance channels. The event spectrum for

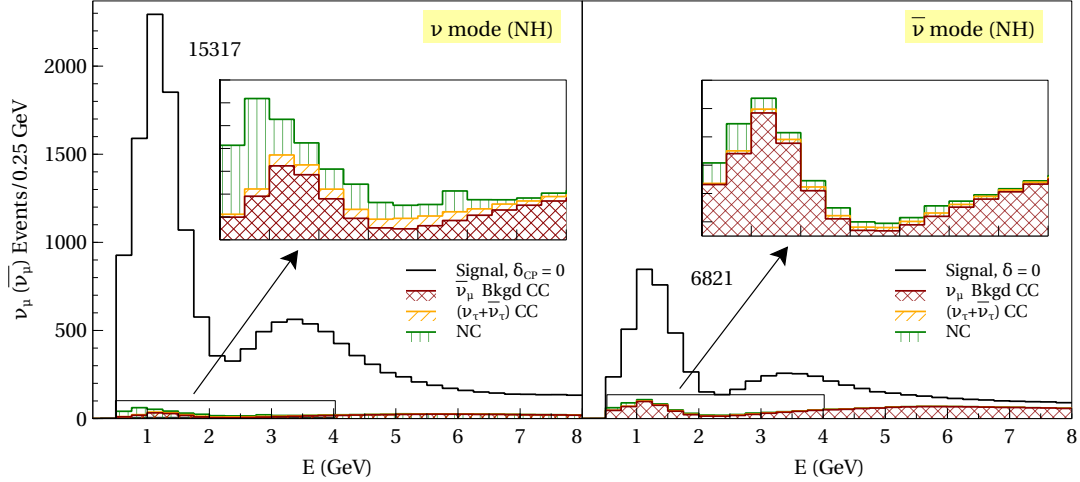


**Figure 7:** Muon (anti-)neutrino disappearance event spectrum with a 40 kt DUNE far detector for the combination of LE 1.1 MW beam, LE 2.2 MW beam and 2<sup>nd</sup> maxima 3 MW beam for  $\delta = 0$ . The runtime is split equally among the three beams (5 yr each) and distributed evenly between neutrino and antineutrino modes (2.5 yr +2.5 yr).

option (c) is shown in Fig. 6 and Fig. 7. Fig. 6 corresponds to  $\nu_e$  appearance events while Fig. 7 depicts  $\nu_\mu$  disappearance events. In general, one notes that the events are peaked at the value of energy where the flux is largest - for 80 GeV LE beam, the events peak around 2–3 GeV while for 8 GeV beam, it is around 0.8–0.9 GeV. The  $\delta$ -dependence of the event spectrum can be understood from the  $\delta$  dependence of the probabilities.

The signal for  $\nu_e$  appearance is an excess of charged-current (CC)  $\nu_e$  and  $\bar{\nu}_e$  interactions over the expected background in the far detector. The background to  $\nu_e$  appearance is composed of

- Beam ( $\nu_e + \bar{\nu}_e$ ) CC : CC interactions of  $\nu_e$  and  $\bar{\nu}_e$  intrinsic to the beam;
- ( $\nu_\tau + \bar{\nu}_\tau$ ) CC :  $\nu_\tau$  and  $\bar{\nu}_\tau$  CC events in which the  $\tau$ 's decay leptonically into electrons/positrons.
- ( $\nu_\mu + \bar{\nu}_\mu$ ) CC : misidentified  $\nu_\mu$  and  $\bar{\nu}_\mu$  CC events;
- NC : neutral current backgrounds

It should be noted that though NC and  $\nu_\tau$  backgrounds are due to interactions of higher-energy neutrinos, they contribute to backgrounds mainly at lower energies which impacts sensitivity to CP violation.

## 5 Analysis procedure

To estimate the sensitivities of DUNE to CP violation, MH, and octant of  $\theta_{23}$ , we perform the standard  $\chi^2$  analysis. Even though all results are produced numerically with the help of GLOBES software, in order to gain insight, let us examine the analytical form of the  $\chi^2$

Beam options	$\nu_\mu \rightarrow \nu_e$		$\bar{\nu}_\mu \rightarrow \bar{\nu}_e$		$\nu_\mu \rightarrow \nu_\mu$	$\bar{\nu}_\mu \rightarrow \bar{\nu}_\mu$
	NH	IH	NH	IH	NH	NH
<b>(a) LE, 1.1 MW + LE, 2.2 MW</b>						
Signal $\delta = 0$	3222	1759	859	1303	13415	6158
Signal $\delta = \pi/2$	2727	1481	928	1463		
Signal $\delta = -\pi/2$	3784	2167	742	1130		
Bkgd ( $\bar{\nu}_e + \nu_e$ ) CC	446	461	227	224		
Bkgd ( $\bar{\nu}_\mu + \nu_\mu$ ) CC	6	6	4	3		
Bkgd ( $\bar{\nu}_\tau + \nu_\tau$ ) CC	43	44	25	25	61	38
Bkgd NC	55	55	27	27	155	81
Bkgd $\nu_\mu$ CC						1536
Bkgd $\bar{\nu}_\mu$ CC					8617	
<b>(b) 2<sup>nd</sup> maxima, 3 MW</b>						
Signal $\delta = 0$	208	121	40	82	1902	663
Signal $\delta = \pi/2$	178	93	45	85		
Signal $\delta = -\pi/2$	292	175	30	58		
Bkgd ( $\bar{\nu}_e + \nu_e$ ) CC	37	38	13	12		
Bkgd ( $\bar{\nu}_\mu + \nu_\mu$ ) CC	1	1	1	1		
Bkgd ( $\bar{\nu}_\tau + \nu_\tau$ ) CC	0	0	0	0	0	0
Bkgd NC	4	4	1	1	11	5
Bkgd $\nu_\mu$ CC						27
Bkgd $\bar{\nu}_\mu$ CC					8	
<b>(c) LE, 1.1 MW + LE, 2.2 MW + 2<sup>nd</sup> maxima, 3 MW</b>						
Signal $\delta = 0$	3430	1880	899	1384	15317	6821
Signal $\delta = \pi/2$	2904	1574	973	1548		
Signal $\delta = -\pi/2$	4076	2342	772	1188		
Bkgd ( $\bar{\nu}_e + \nu_e$ ) CC	483	499	239	236		
Bkgd ( $\bar{\nu}_\mu + \nu_\mu$ ) CC	7	7	4	4		
Bkgd ( $\bar{\nu}_\tau + \nu_\tau$ ) CC	43	44	25	25	61	38
Bkgd NC	59	59	28	28	166	86
Bkgd $\nu_\mu$ CC						1563
Bkgd $\bar{\nu}_\mu$ CC					555	

**Table 4:** Total number of event rates for different beamtune combinations.

relevant for each of the mentioned unknowns.

**Sensitivity to CP violation :-** Including only statistical effects, the  $\chi^2$  for CP violation sensitivity for a given oscillation channel (say  $\nu_\mu \rightarrow \nu_e$ ) is given by [38, 52]

$$\chi^2 \equiv \min_{\delta_{test}} \sum_{i=1}^x \sum_{j=\nu, \bar{\nu}} \frac{[N_{true}^{i,j}(\delta_{true}) - N_{test}^{i,j}(\delta_{test} = 0, \pi)]^2}{N_{true}^{i,j}(\delta_{true})} \quad (14)$$

where  $N_{true}^{i,j}$  and  $N_{test}^{i,j}$  are the number of true and test events in the  $\{i, j\}$ -th bin respectively <sup>2</sup>. The index  $i$  corresponds to energy bins ( $i = 1 \rightarrow x$ , the number of bins depends upon the particular experiment under consideration. For the case of DUNE, there are 64 bins of width 125 MeV in 0 – 8 GeV and 7 unequal bins in 8 – 20 GeV.  $j$  is being summed over the neutrino and anti-neutrino contribution. In order to determine the  $\chi^2$  that concerns the sensitivity to CP violation, the test value of phase ( $\delta$ ) is assumed to be 0 or  $\pi$  and the  $\chi^2$  for any true value of phase ( $\delta$ ) in the full range of  $[-\pi, \pi]$  is computed.

The characteristic double peak shape of the curves are expected since the sensitivity drops to zero at the CP conserving values while it is maximum at the maximal CP violating values ( $\delta = \pm\pi/2$ ). The  $\chi^2$  is computed as given in Eq. 14 for a given set of true values by minimizing over the test parameters and this procedure is repeated for all possible true values

---

<sup>2</sup> $N_\sigma = \sqrt{\Delta\chi^2}$ .  $\Delta\chi^2 = \chi^2$  as we have not included any fluctuations in simulated data. This is the Pearson's definition of  $\chi^2$  [53]. For large sample size, the other definition using log-likelihood also yields similar results.

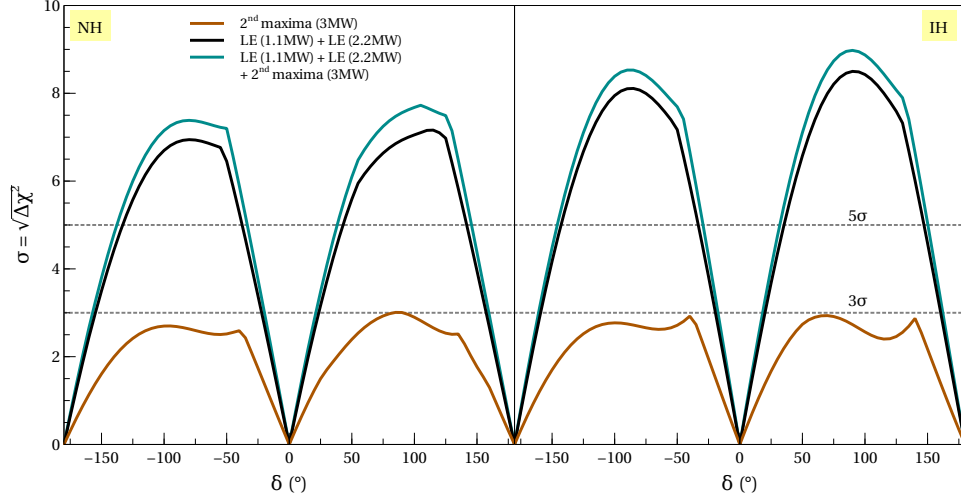


**Figure 8:** Sensitivity to CP violation as a function of  $\delta$ . The three curves correspond to  $2^{nd}$  maxima 3MW beam (2.5yr  $\nu$  + 2.5yr  $\bar{\nu}$ ), LE 1.1 MW beam (2.5yr  $\nu$  + 2.5yr  $\bar{\nu}$ ) + LE 2.2 MW beam (2.5yr  $\nu$  + 2.5yr  $\bar{\nu}$ ) and LE 1.1 MW beam (2.5yr  $\nu$  + 2.5yr  $\bar{\nu}$ ) + LE 2.2 MW beam (2.5yr  $\nu$  + 2.5yr  $\bar{\nu}$ ) +  $2^{nd}$  maxima 3MW beam (2.5yr  $\nu$  + 2.5yr  $\bar{\nu}$ ).

listed in Table 1. Some general remarks relevant for computation of  $\chi^2$  for this and other unknowns are in order. We do not marginalise over the standard oscillation parameters except  $\delta$  whose true value is unknown. It should be noted that the total  $\chi^2$  is a sum of contributions from the two channels ( $\nu_\mu \rightarrow \nu_e$  and  $\nu_\mu \rightarrow \nu_\mu$ ).

**Sensitivity to the MH :-** As is known, the question of MH is a binary one, i.e., there can only be two possibilities for the true choice of hierarchy (NH or IH) and one would like to decipher the sensitivity of DUNE to figure out the correct MH.

In order to understand the features of the sensitivity plots (considering the true hierarchy as NH or IH), we give a statistical definition of  $\chi^2$  as follows [54].

$$\chi^2 \equiv \min_{\delta_{test}} \sum_{i=1}^x \sum_{j=\nu, \bar{\nu}} \frac{[N_{NH}^{i,j}(\delta_{true}) - N_{IH}^{i,j}(\delta_{test})]^2}{N_{NH}^{i,j}(\delta_{true})} \quad (15)$$

where the true hierarchy is taken to be NH.  $N_{NH}^{i,j}$  and  $N_{IH}^{i,j}$  are the number of NH and IH events in the  $\{i, j\}$ -th bin respectively. The index  $i$  corresponds to energy bins ( $i = 1 \rightarrow x$ , the number of bins depends upon the particular experiment under consideration. For the case of DUNE, there are 64 bins of width 125 MeV in 0 – 8 GeV and 7 unequal bins in 8 – 20 GeV.  $j$  is being summed over the neutrino and anti-neutrino contribution. The  $\chi^2$  is computed as given in Eq. 15 for a given set of true values by minimizing over the test parameters and this procedure is repeated for all possible true values listed in Table 1. The shape of the sensitivity curves can be explained using analytic form of probabilities [52, 54].

**Sensitivity to the octant of  $\theta_{23}$  :-** It is important to determine the value of  $\sin^2 \theta_{23}$  with sufficient precision to determine the octant of  $\theta_{23}$ . A combination of  $\nu_e$  appearance (which is sensitive to  $\sin^2 \theta_{23}$ ) and  $\nu_\mu$  disappearance (sensitive to  $\sin^2 2\theta_{23}$ ) measurements would

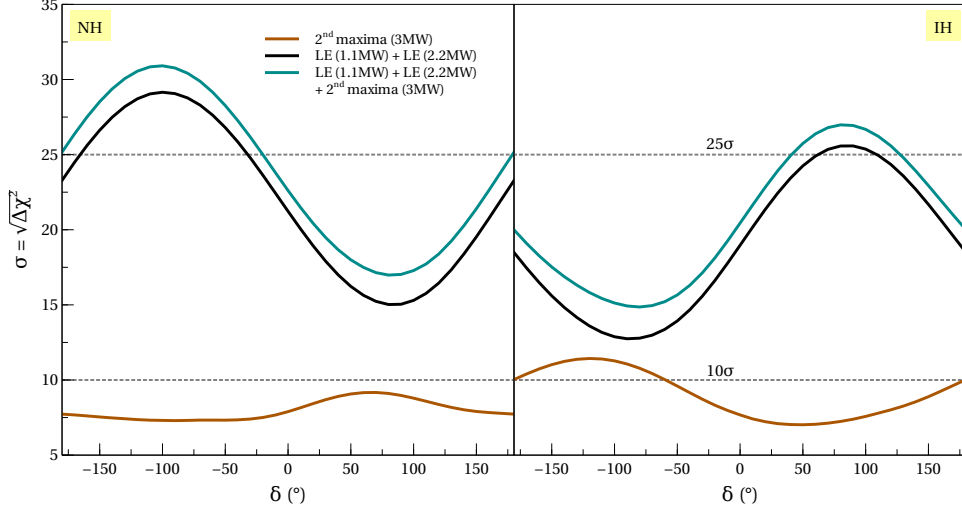


**Figure 9:** Sensitivity to MH as a function of  $\delta$ . The three curves correspond to  $2^{nd}$  maxima 3MW beam (2.5yr  $\nu + 2.5$ yr  $\bar{\nu}$ ), LE 1.1 MW beam (2.5yr  $\nu + 2.5$ yr  $\bar{\nu}$ ) + LE 2.2 MW beam (2.5yr  $\nu + 2.5$ yr  $\bar{\nu}$ ) and LE 1.1 MW beam (2.5yr  $\nu + 2.5$ yr  $\bar{\nu}$ ) + LE 2.2 MW beam (2.5yr  $\nu + 2.5$ yr  $\bar{\nu}$ ) +  $2^{nd}$  maxima 3MW beam (2.5yr  $\nu + 2.5$ yr  $\bar{\nu}$ ).

allow us to probe both maximal mixing and the octant of  $\theta_{23}$ . The  $\Delta\chi^2$  is defined as [8]

$$\Delta\chi_{octant}^2 = |\chi_{\theta_{23}^{test} > 45^\circ}^2 - \chi_{\theta_{23}^{test} < 45^\circ}^2| \quad (16)$$

where the value of  $\theta_{23}$  in the wrong octant is constrained only to have a value within the wrong octant (i.e., it is not required to have the same value of  $\sin^2 2\theta_{23}$  as the true value).

## 6 Results

One of the primary objectives of DUNE is to ascertain whether CP is violated in the leptonic sector within the context of the standard three flavor mixing scenario. In Fig. 8, we depict CP violation sensitivity as a function of  $\delta$  for different beam tune combinations. The largest sensitivity to CP violation occurs at  $\delta = \pm\pi/2$ . This is expected because the difference between the event rates at  $\delta = \pm\pi/2$  (maximal CP violating values) and  $\delta = 0$  or  $\pi$  (CP conserving values) is the largest. The contribution from the  $2^{nd}$  maxima beam (brown curve) stays below  $3\sigma$  level for all values of CP phase. The contribution from LE 1.1 MW and LE 2.2 MW beam taken together is shown as black curve and for the considered exposure, the sensitivity lies above  $3\sigma$  level for favourable values of the CP phase ( $\sim 75 - 80\%$ ). The combination LE 1.1 MW and LE 2.2 MW beam along with  $2^{nd}$  maxima beam *improves the sensitivity to CP violation* near the maximal CP violating values. This holds irrespective of the choice of hierarchy.

In Fig. 9, we show sensitivity to the MH as a function of  $\delta$ . Here again, we get better results for the LE beam as compared to the  $2^{nd}$  maxima beam. However, when we consider the combination of beam tunes (LE 1.1 MW, LE 2.2 MW and  $2^{nd}$  maxima), we notice an *overall improvement in the sensitivity to MH* for all values of  $\delta$ . With the exposure considered, one can discern the MH sensitivity above  $10\sigma$  level for the LE beam combination and for the combination of LE with the  $2^{nd}$  maxima.

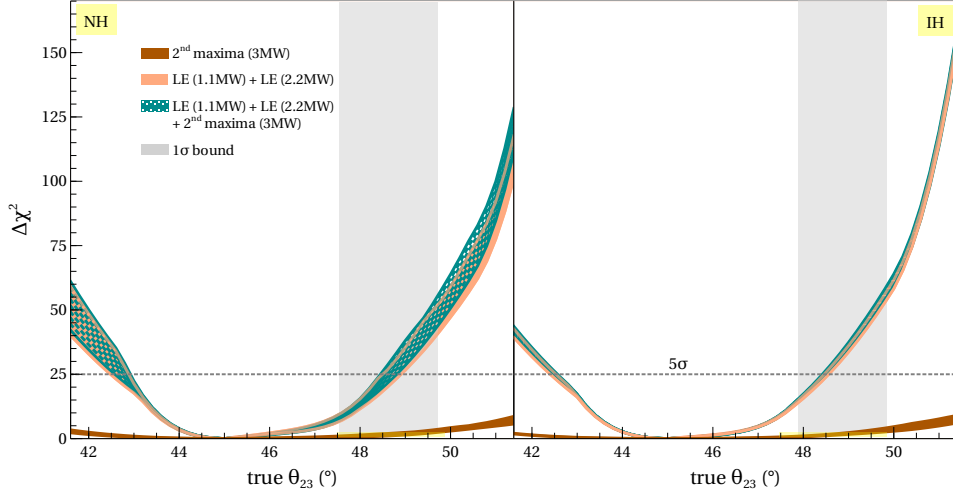
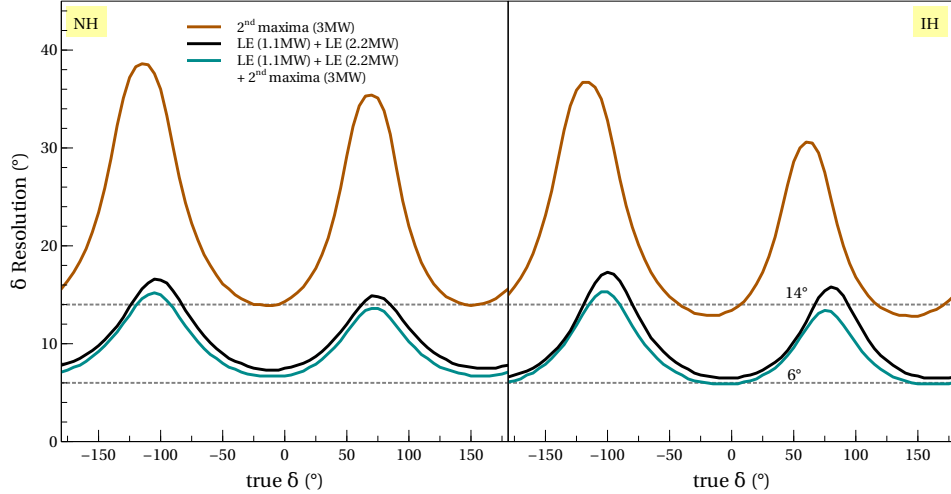


**Figure 10:** The significance with which DUNE can resolve the  $\theta_{23}$  octant as a function of the true value of  $\theta_{23}$  for different combinations of beams. The shaded band around the curve represents the range in sensitivity due to potential variations in the true value of  $\delta$ . The grey shaded regions indicate the current  $1\sigma$  bounds on the value of  $\theta_{23}$  from a global fit.

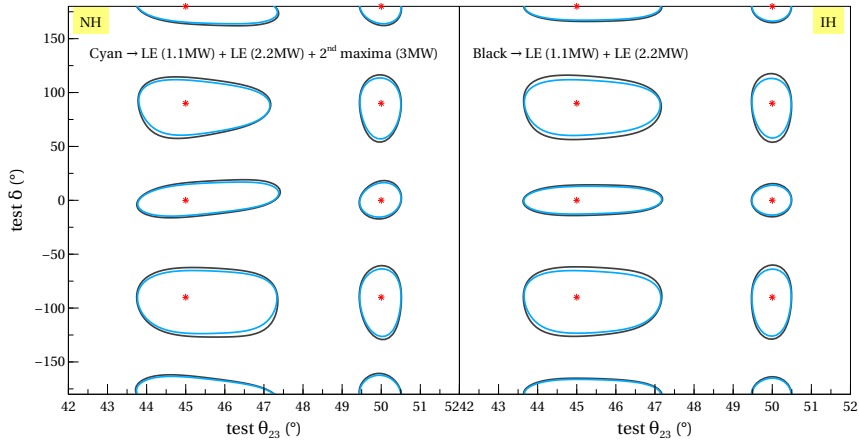
DUNE will not only address questions pertaining to CP violation and neutrino MH, but also improve the precision on key parameters ( $\sin^2 \theta_{23}$  and the octant of  $\theta_{23}$ ,  $\delta$ ,  $\sin^2 2\theta_{13}$  and  $\Delta m_{31}^2$ ) entering the oscillation framework. It is crucial to determine the value of  $\sin^2 \theta_{23}$  with sufficient precision to determine the octant. The sensitivity of determining the octant of  $\theta_{23}$  as a function of true value of  $\theta_{23}$  for different beam combinations is shown in Fig. 10 for NH and IH. Adding the 8 GeV beam data to 80 GeV data at DUNE *improves the sensitivity to resolution of the  $\theta_{23}$  octant degeneracy*. The width of each curve is due to the unknown CP phase and covers all possible true  $\delta$  values. The grey shaded regions indicate the current  $1\sigma$  bounds on the value of  $\theta_{23}$  from a global fit [3]. In this fit, muon neutrino disappearance contributes to the precision on  $\sin^2 2\theta_{23}$  while the electron neutrino appearance data provides information on the  $\theta_{23}$  octant. A  $5\sigma$  determination of the octant of  $\theta_{23}$  will be possible for at least 90% of true values of  $\delta$  for  $42.5^\circ < \theta_{23} < 49^\circ$  for NH. Most of the sensitivity comes from the LE data because the  $2^{nd}$  maximum does not provide any added sensitivity to the octant determination. Significant improvement can be achieved with high mass far detector (such as a 200 kt WC detector).

Fig. 11 shows one-dimensional resolution on the measurement of  $\delta$  (see [13, 55] for details) for simultaneous low-energy beams to the far detector with a range of exposure to beams with energies 8 GeV - 80 GeV, varying from 600 kt-MW-yr to 1260 kt-MW-yr. The low energy ( $2^{nd}$  maxima) beams in conjunction with standard LE beam at DUNE, leads to *some improvement in  $\delta$  resolution* (the  $\delta$  resolution is  $\sim 6^\circ$  for  $\delta = 0^\circ$  and  $\pm 180^\circ$  and  $\sim 14^\circ$  for  $\delta = 90^\circ$  for IH) for almost all true values of  $\delta$  (irrespective of the choice of hierarchy).

The  $1\sigma$  contours from a two-dimensional fit to  $\theta_{23}$  and  $\delta$  with external constraint on  $\theta_{13}$  for the combinations considered in the present work are shown in Fig. 12. Additionally, data from the LE and  $2^{nd}$  maxima beam place independent constraints on other neutrino oscillation parameters as well.



**Figure 11:** Resolution on the measurement of  $\delta$  as a function of the true value of  $\delta$  for various beam combinations at DUNE.



**Figure 12:**  $1\sigma$  contour plots from a two-dimensional fit for  $\theta_{23}$  and  $\delta$  for the different beamtune combinations. Fit results for various possible true values of  $\delta = 0, \pm\pi/2, \pi$  are shown.

## 7 Conclusion

The present study highlights the importance of second oscillation maximum in  $\nu_\mu \rightarrow \nu_e$  channel and its impact on addressing the current unknowns in the neutrino oscillation physics. The accelerator-based long baseline neutrino program aims to constrain the parameters of the mixing matrix (or find deviations from the standard paradigm) through extremely precise measurements of flavour oscillations with systematic uncertainties well within percent level. The idea of exploring physics at tertiary maxima of  $P_{\mu e}$  in the context of various experiments is of paramount importance as it allows for complete underpinning of the standard three flavour oscillation framework since it allows us to study wide  $L/E$  range (for a fixed baseline).

The usefulness of observing the second oscillation maximum can be understood in terms

of an argument based on CP asymmetries. In order to observe a signal for CP violation in the leptonic sector, one needs to measure the CP conjugate channels ( $\nu_\mu \rightarrow \nu_e$  and  $\bar{\nu}_\mu \rightarrow \bar{\nu}_e$ ). The interference term has the CP violating parameter  $\delta$  and should be larger (ideally) compared to the other two terms (solar and atmospheric). For the measured value of  $\theta_{13}$ , the interference term is large compared to the other two terms. The CP asymmetry is larger at the second oscillation maximum since  $A_{\mu e}^{CP} \simeq 0.75 \sin \delta$  (at  $L/E \simeq 1500$  km/GeV) and  $A_{\mu e}^{CP} \simeq 0.3 \sin \delta$  (at  $L/E \simeq 500$  km/GeV)]. This implies significantly higher sensitivity to observe CP violation. Now, if neutrino energy is held fixed, the baseline has to be about three times larger than for the first oscillation maximum. But, this leads to a reduction in statistics by an order of magnitude. However, the other potentially viable option is to use a very intense neutrino beam from a multi-MW proton beam. In the recent times, there is an upsurge in activity relating to analyzing the role of second oscillation maximum in the context of ESS $\nu$ SB (which covers the second oscillation maximum using 5MW proton linac as neutrino source and WC detector placed at  $\sim 500$  km away) and T2HKK both within and beyond the standard three flavour mixing paradigm. However, a detailed and comprehensive study investigating the role of second oscillation maximum has not yet been carried out in the context of DUNE.

Our experimental setup comprises of LBNF/DUNE using a neutrino beam covering the 2<sup>nd</sup> maxima in conjunction with the standard CP optimized wide-band beam currently under design [8]. The neutrino beam at the second maxima is generated using a 3 MW, 8 GeV proton beam which could be generated by the PIP-III superconducting linac option [45].

The main results of our sensitivity studies with the considered beam combination are contained in Figs. 8-12. The second maximum data along with the data from first oscillation maximum aids in improving the sensitivity to CP Violation, MH and octant of  $\theta_{23}$  (see Figs. 8, 9 and 10). One of our key results pertains to some improvement in resolution of  $\delta$  (see Fig. 11). The resolution of  $\delta$  is  $\sim 6^\circ$  for  $\delta = 0^\circ$  and  $\pm 180^\circ$  and  $\sim 14^\circ$  for  $\delta = 90^\circ$  for IH. The low energy (2<sup>nd</sup> maxima) beams in conjunction with standard LE beam at DUNE, leads to an *improvement in  $\delta$  resolution* for almost all true values of  $\delta$  (irrespective of the choice of hierarchy). We also show the  $1\sigma$  contours from a two-dimensional fit to  $\theta_{23}$  and  $\delta$  for the beamtune combinations considered in the present work (see Fig. 12).

Further improvements may be possible with improved energy resolution (using different detector technology like WC detector or improvements in LArTPC reconstruction) and increased efficiency at the 2<sup>nd</sup> maxima.

## Acknowledgements

JR and SS thank the University Grants Commission for financial support in the form of research fellowships. This material is based upon work supported by the U.S. Department of Energy, Office of Science, Office of High Energy Physics under contract number DE-SC0012704; the Indian funding from University Grants Commission under the second phase of University with Potential of Excellence (UPE II) at JNU and Department of Science and Technology under DST-PURSE at JNU. This work has received partial funding from the European Union's Horizon 2020 research and innovation programme under the Marie Sklodowska-Curie grant agreement No 690575 and 674896.

## References

- [1] B. Pontecorvo, Sov. Phys. JETP **26**, 984 (1968).
- [2] T. Kajita and A. B. McDonald, *For the discovery of neutrino oscillations, which shows that neutrinos have mass*, the Nobel Prize in Physics 2015.
- [3] P. de Salas, D. Forero, S. Gariazzo, P. Martínez-Miravé, O. Mena, C. Ternes, M. Tórtola, and J. Valle (2020), 2006.11237.
- [4] I. Esteban, M. Gonzalez-Garcia, M. Maltoni, T. Schwetz, and A. Zhou, JHEP **09**, 178 (2020), 2007.14792.
- [5] C. H. Albright and M.-C. Chen, Phys. Rev. **D74**, 113006 (2006), hep-ph/0608137.
- [6] M. Fukugita and T. Yanagida, Phys. Lett. **B174**, 45 (1986).
- [7] C. Adams *et al.* (LBNE Collaboration), ArXiv e-prints (2013), 1307.7335.
- [8] R. Acciarri *et al.* (DUNE) (2015), 1512.06148.
- [9] R. Acciarri *et al.* (DUNE) (2016), 1601.05471.
- [10] M. Bass *et al.* (LBNE Collaboration), Phys. Rev. **D91**, 052015 (2015), 1311.0212.
- [11] M. Bishai, M. Diwan, S. Kettell, J. Stewart, B. Viren, E. Worcester, R. Tschirhart, and L. Whitehead, in *Proceedings, 2013 Community Summer Study on the Future of U.S. Particle Physics: Snowmass on the Mississippi (CSS2013): Minneapolis, MN, USA, July 29-August 6, 2013* (2013), 1307.0807, URL <http://www.slac.stanford.edu/econf/C1307292/docs/submittedArxivFiles/1307.0807.pdf>.
- [12] X. Qian, J. J. Ling, R. D. McKeown, W. Wang, E. Worcester, and C. Zhang, in *Proceedings, 2013 Community Summer Study on the Future of U.S. Particle Physics: Snowmass on the Mississippi (CSS2013): Minneapolis, MN, USA, July 29-August 6, 2013* (2013), 1307.7406, URL <http://www.slac.stanford.edu/econf/C1307292/docs/submittedArxivFiles/1307.7406.pdf>.
- [13] P. Coloma, H. Minakata, and S. J. Parke, Phys. Rev. D **90**, 093003 (2014), 1406.2551.
- [14] P. Huber and J. Kopp, JHEP **03**, 013 (2011), [Erratum: JHEP05,024(2011)], 1010.3706.
- [15] E. Baussan *et al.* (ESSnuSB), Nucl. Phys. **B885**, 127 (2014), 1309.7022.
- [16] E. Wildner *et al.*, Adv. High Energy Phys. **2016**, 8640493 (2016), 1510.00493.
- [17] M. Blennow, E. Fernandez-Martinez, T. Ota, and S. Rosauero-Alcaraz, Eur. Phys. J. C **80**(3), 190 (2020), 1912.04309.
- [18] S. K. Agarwalla, S. Choubey, and S. Prakash, Journal of High Energy Physics **2014**(12) (2014), ISSN 1029-8479, URL [http://dx.doi.org/10.1007/JHEP12\(2014\)020](http://dx.doi.org/10.1007/JHEP12(2014)020).

- [19] K. Chakraborty, S. Goswami, C. Gupta, and T. Thakore, Journal of High Energy Physics **2019**(5) (2019), ISSN 1029-8479, URL [http://dx.doi.org/10.1007/JHEP05\(2019\)137](http://dx.doi.org/10.1007/JHEP05(2019)137).
- [20] M. Ghosh and T. Ohlsson, Mod. Phys. Lett. A **35**(05), 2050058 (2020), 1906.05779.
- [21] M. Ghosh and O. B. O. E. Wp6, PoS **NuFact2019**, 038 (2020).
- [22] J. Cao, M. He, Z.-L. Hou, H.-T. Jing, Y.-F. Li, Z.-H. Li, Y.-P. Song, J.-Y. Tang, Y.-F. Wang, Q.-F. Wu, and et al., Physical Review Special Topics - Accelerators and Beams **17**(9) (2014), ISSN 1098-4402, URL <http://dx.doi.org/10.1103/PhysRevSTAB.17.090101>.
- [23] J. Tang, S. Vihonen, and T.-C. Wang, JHEP **12**, 130 (2019), 1909.01548.
- [24] K. Hagiwara and N. Okamura, Journal of High Energy Physics **2008**(01), 022?022 (2008), ISSN 1029-8479, URL <http://dx.doi.org/10.1088/1126-6708/2008/01/022>.
- [25] S. Choubey, M. Ghosh, D. Kempe, and T. Ohlsson (2020), 2010.16334.
- [26] K. Chakraborty, D. Dutta, S. Goswami, and D. Pramanik (2020), 2012.04958.
- [27] J. Beringer *et al.* (Particle Data Group), Phys. Rev. **D86**, 010001 (2012).
- [28] C. Giunti, Physics Letters B **686**(1), 41 (2010), ISSN 0370-2693, URL <http://www.sciencedirect.com/science/article/pii/S0370269310001942>.
- [29] A. de Gouvêa, K. J. Kelly, G. V. Stenico, and P. Pasquini, Phys. Rev. D **100**, 016004 (2019), URL <https://link.aps.org/doi/10.1103/PhysRevD.100.016004>.
- [30] A. De Gouvêa, K. J. Kelly, G. Stenico, and P. Pasquini, Phys. Rev. D **100**(1), 016004 (2019), 1904.07265.
- [31] A. Ghoshal, A. Giarnetti, and D. Meloni, JHEP **12**, 126 (2019), 1906.06212.
- [32] J. Rout, S. Roy, M. Masud, M. Bishai, and P. Mehta (2020), 2009.05061.
- [33] W. Marciano and Z. Parsa, Nucl. Phys. Proc. Suppl. **221**, 166 (2011), hep-ph/0610258.
- [34] A. Cervera, A. Donini, M. Gavela, J. Gomez Cadenas, P. Hernandez, *et al.*, Nucl.Phys. **B579**, 17 (2000), hep-ph/0002108.
- [35] M. Freund, Phys. Rev. **D64**, 053003 (2001), hep-ph/0103300.
- [36] E. K. Akhmedov, R. Johansson, M. Lindner, T. Ohlsson, and T. Schwetz, JHEP **0404**, 078 (2004), hep-ph/0402175.
- [37] E. K. Akhmedov, Phys. Scripta **T121**, 65 (2005), hep-ph/0412029.
- [38] M. Masud, A. Chatterjee, and P. Mehta, J. Phys. **G43**(9), 095005 (2016), 1510.08261.
- [39] C. Jarlskog, Phys. Lett. **B609**, 323 (2005), hep-ph/0412288.

- [40] S. P. Mikheev and A. Y. Smirnov, *Sov. Phys. Usp.* **30**, 759 (1987).
- [41] L. Wolfenstein, *Phys. Rev.* **D17**, 2369 (1978).
- [42] H. Nunokawa, S. J. Parke, and J. W. F. Valle, *Prog. Part. Nucl. Phys.* **60**, 338 (2008), 0710.0554.
- [43] J. Rout, M. Masud, and P. Mehta, *Phys. Rev.* **D95**(7), 075035 (2017), 1702.02163.
- [44] *Dune fluxes* (2017), URL <http://home.fnal.gov/~ljf26/DUNEFluxes/>.
- [45] *Proton improvement plan iii* (2015), URL <http://home.fnal.gov/~prebys/misc/PIP-III/>.
- [46] T. Alion *et al.* (DUNE) (2016), 1606.09550.
- [47] R. Acciarri *et al.* (DUNE) (2016), 1601.02984.
- [48] P. Huber, M. Lindner, and W. Winter, *Comput. Phys. Commun.* **167**, 195 (2005), hep-ph/0407333.
- [49] P. Huber, J. Kopp, M. Lindner, M. Rolinec, and W. Winter, *Comput. Phys. Commun.* **177**, 432 (2007), hep-ph/0701187.
- [50] A. M. Dziewonski and D. L. Anderson, *Phys. Earth Planet. Interiors* **25**, 297 (1981).
- [51] V. De Romeri, E. Fernandez-Martinez, and M. Sorel, *JHEP* **09**, 030 (2016), 1607.00293.
- [52] M. Masud and P. Mehta, *Phys. Rev.* **D94**, 013014 (2016), 1603.01380.
- [53] X. Qian, A. Tan, W. Wang, J. J. Ling, R. D. McKeown, and C. Zhang, *Phys. Rev.* **D86**, 113011 (2012), 1210.3651.
- [54] M. Masud and P. Mehta, *Phys. Rev.* **D94**(5), 053007 (2016), 1606.05662.
- [55] P. Coloma, A. Donini, E. Fernandez-Martinez, and P. Hernandez, *JHEP* **06**, 073 (2012), 1203.5651.